Dalton Transactions

Accepted Manuscript

ROYAL SOCIETY OF CHEMISTRY

www.rsc.org/dalton

Dalton Transactions

ARTICLE

Mechanistic understanding of the CoO-catalyzed hydrogen desorption from a $LiBH_4{\cdot}NH_3$-3LiH system†

Received 00th January 20xx,
Accepted 00th January 20xx

DOI: 10.1039/x0xx00000x

www.rsc.org/

Yi Zhang,[a] Yongfeng Liu,[a,b]* Xin Zhang,[a] You Li,[a] Mingxia Gao,[a] and Hongge Pan[a]

The addition of a minor quantity of CoO significantly reduces the dehydrogenation temperature, accelerates the dehydrogenation rate and increases the hydrogen purity of the $LiBH_4{\cdot}NH_3$-3LiH system. The $LiBH_4{\cdot}NH_3$-3LiH-0.1CoO sample exhibits the optimal dehydrogenation properties because it releases 8.5 wt% of hydrogen below 250 °C, which is approximately 90 °C lower than that of the pristine sample. At 200 °C, approximately 8.0 wt% of hydrogen is released from the $LiBH_4{\cdot}NH_3$-3LiH-0.1CoO sample within 100 min, whereas only 4.1 wt% is released from the pristine sample under identical conditions. The EXAFS analyses reveal that upon heating, CoO is first reduced to metallic Co at 130 °C and then partially combines with B to form a Co-B species. The *in situ* formed Co and Co-B are finely dispersed in the dehydrogenated intermediates, and they play critical roles as active catalysts in favour of breaking the B-H bonds of the Li-B-N-H species. This effectively decreases the thermodynamic and kinetic barriers of the dehydrogenation reaction of the $LiBH_4{\cdot}NH_3$-3LiH system.

Introduction

In considering the rapid depletion of fossil fuels and the increasing concerns concerning environmental pollution, it is imperative to develop a renewable, efficient and eco-friendly energy source.[1] Hydrogen is regarded as an ideal alternative to fossil fuels in future energy systems.[2-3] However, hydrogen storage is still one of the key challenges in developing hydrogen-based energy. Significant efforts dedicated to the development of solid-state hydrogen storage systems with high gravimetric and volumetric hydrogen densities have been made, especially for complex hydrides including metal borohydrides, alanates and amides/imides.[4-15] However, the rigorous conditions required for reversible hydrogen storage arising from their thermodynamic and kinetic limitations remains an unsolved problem after decades of exploration. For example, lithium borohydride, with a hydrogen content of 18.4 wt%, can only be partially rehydrided under 350 bar of hydrogen at 500 °C or at 150 bar at 727 °C after decomposing into LiH and B.[16-17] Recently, a novel series of boron-nitrogen-hydrogen compounds with a relatively low decomposition temperature and high hydrogen content were developed. These include amide-borohydride combinations, metal amidoboranes and metal borohydride ammoniates.[18-26] Pinkerton et al. discovered a new quaternary hydride, $Li_3BN_2H_8$, produced by ball milling at ambient temperature or by heating the $2LiNH_2$-$LiBH_4$ mixture above 95 °C, which releases more than 10 wt% hydrogen from an onset temperature of 250 °C.[19] By substituting one H in the NH_3 group in ammonia borane (NH_3BH_3) with a more electron-donating element (*e.g.*, Li or Na), Xiong et al. obtained lithium amidoborane ($LiNH_2BH_3$) and sodium amidoborane ($NaNH_2BH_3$).[21] These newly developed compounds exhibited significantly improved dehydrogenation characteristics, with more than 10 and 7 wt% of hydrogen desorbed from $LiNH_2BH_3$ and $NaNH_2BH_3$, respectively, at approximately 90 °C. In particular, Soloveichik et al. proposed the use of ammonia complexes of metal borohydrides $M(BH_4)_n{\cdot}mNH_3$ as hydrogen storage media to combine the properties of metal hydrides and ammonia borane.[22] As an example, $Mg(BH_4)_2{\cdot}2NH_3$ desorbed 13.1 wt% H_2 at 120-400 °C, exhibiting a distinctly reduced operating temperature for hydrogen desorption with respect to $Mg(BH_4)_2$. The relatively close local interactions between the hydridic ($H^{\delta-}$) and protic ($H^{\delta+}$) atoms bonded to nitrogen and boron, respectively, are believed to be crucial for improving the dehydrogenation properties in these materials.[24-26]

More recently, the use of the monoammoniate of lithium borohydride ($LiBH_4{\cdot}NH_3$), one of the most hydrogen-rich inorganic materials, has received considerable attention for hydrogen storage applications. This material was first synthesized by Hunt and Cowie in 1955,[27] and it has a hydrogen storage content of 17.8 wt%. The crystal structure was determined to be an orthorhombic *Pnma* (No. 62) structure with lattice parameters of a = 5.96910(3) Å, b = 4.46355(8) Å and c = 14.34199(8) Å, with a corresponding cell

[a] State Key Laboratory of Silicon Materials, Key Laboratory of Advanced Materials and Applications for Batteries of Zhejiang Province and Department of Materials Science and Engineering, Zhejiang University, Hangzhou 310027, People's Republic of China. Tel/Fax: +86 571 87952615, E-mail: mselyf@zju.edu.cn
[b] Key Laboratory of Advanced Energy Materials Chemistry (Ministry of Education), Nankai University, Tianjin 300071, People's Republic of China

† Electronic Supplementary Information (ESI) available: EDS mapping of $LiBH_4{\cdot}NH_3$-3LiH-0.1CoO, ^{11}B NMR spectra of $LiBH_4$ and $LiBH_4{\cdot}NH_3$-3LiH-0.1CoO with different treatments. See DOI: 10.1039/x0xx00000x

volume V = 382.119(2) Å^3.[28] The BH-NH distances in $LiBH_4{\cdot}NH_3$ are approximately 2.3-2.5 Å. This suggests dihydrogen bonds exist in this structure. Unfortunately, it was found that $LiBH_4{\cdot}NH_3$ mainly released ammonia rather than hydrogen upon heating under an argon flow, possibly due to the weaker Li-N coordination and stronger B-H bonds.[29] Considerable work has been conducted to improve the dehydrogenation properties of $LiBH_4{\cdot}NH_3$ by the addition of catalysts, nanoconfinement and by creating reactive composites.[29-32] Zheng et al. demonstrated that 17.8 wt% of hydrogen was released from the $CoCl_2$-added $Li(NH_3)_{4/3}BH_4$ below 250 °C in a closed vessel.[29] However, under these conditions, a specially designed isolated system is required for the maintenance of an appropriate ammonia equilibrium vapour pressure and real-time desorption of high-purity hydrogen in practical use. Alternatively, confining $LiBH_4{\cdot}NH_3$ within nanoporous SiO_2 or Al_2O_3 nanoscaffolds significantly suppressed the emission of NH_3 and decreased the onset dehydrogenation temperature.[30,31] For example, the $LiBH_4{\cdot}NH_3$ melt-infiltrated into the Al_2O_3 nanoscaffolds detached 12.8 wt% hydrogen at 230 °C, accounting for 91 mol% of the total amount of the gas released.[30] In addition, metal hydrides were also found to be effective in promoting the dehydrogenation of $LiBH_4{\cdot}NH_3$. Guo et al. reported that the $LiBH_4{\cdot}NH_3$-3LiH mixture liberated more than 10 wt% hydrogen at 60-600 °C without any NH_3 detected.[32] Unfortunately, the majority of hydrogen desorption occurred above 200 ºC, which is still too high for practical applications. Therefore, further reduction in the dehydrogenation temperature of the $LiBH_4{\cdot}NH_3$-3LiH system is highly desired.

In this work, CoO, which has been recently proved to be quite effective in catalyzing hydrogen desorption from the $2LiNH_2$-$LiBH_4$ system,[33-35] was introduced to the $LiBH_4{\cdot}NH_3$-3LiH system as a catalyst precursor to achieve significantly reduced dehydrogenation temperatures. Five samples of $LiBH_4{\cdot}NH_3$-3LiH-*x*CoO with *x* = 0, 0.01, 0.05, 0.10 and 0.15 were designed and prepared. The qualitative and quantitative dehydrogenation behaviour of the as-prepared $LiBH_4{\cdot}NH_3$-3LiH-xCoO systems were systematically investigated, and the role of CoO in the dehydrogenation was discussed in detail.

Experimental

$LiBH_4$ (98%, Strem Chemical), CoO (99%, Alfa Aesar) and anhydrous ammonia gas (NH_3, Sinopharm) were used as received. The monoammoniate of lithium borohydride ($LiBH_4{\cdot}NH_3$) was prepared by first exposing $LiBH_4$ to an anhydrous NH_3 atmosphere at ambient temperature and then heating the saturated ammoniate. In a typical experiment, NH_3 at a pressure of 5 bar was introduced to a vessel containing pristine $LiBH_4$ powder and maintained for several minutes. The vessel was then heated at 60 and 80 °C for 2 h, respectively, in a water bath and evacuated for 10 min every 1 h to yield $LiBH_4{\cdot}NH_3$. The target $LiBH_4{\cdot}NH_3$-3LiH-*x*CoO samples with various compositions (*x* = 0, 0.01, 0.05, 0.10 and 0.15) were prepared by hand milling the corresponding chemicals using a mortar and pestle for 10 min. Approximately 50 mg of mixture was milled each time, and the resultant product displayed roughly uniform element distribution (Fig. S1, ESI†). All sample handling was conducted in a Schlenk apparatus or a glove box (MBRAUN 200B, Germany) filled with high purity Ar (H_2O < 1 ppm; O_2 < 1 ppm).

The temperature-dependence of gaseous desorption was evaluated using a homemade temperature-programmed-desorption (TPD) system. The gaseous composition that evolved from the sample was examined by mass spectrometry (MS, Hiden QIC-20). Approximately 20 mg of sample was gradually heated from room temperature to 600 ºC at a ramping rate of 2 ºC min^{-1} under an argon flow of 20 mL min^{-1}. Quantitative measurements of gaseous desorption were performed on a homemade Sievert-type apparatus. In this experiment, 100 mg of sample was loaded into a stainless steel reactor and vacuumed prior to heating. The sample was heated to a desired temperature at 2 ºC min^{-1}. Differential scanning calorimetry (DSC) was conducted on a Netzsch DSC 200 F3 unit. Approximately 2 mg of sample was heated in an Al_2O_3 crucible from room temperature to 500 ºC at 2 ºC min^{-1}.

The phase structures present in samples were identified by means of powder X-ray diffraction on a PANalytical X'Pert diffractometer equipped with Cu Kα radiation (40 kV and 40 mA). Data were collected from 10 to 90° (2ϑ) with a step increment of 0.05° at ambient temperature. A homemade container was applied to prevent water and oxygen contamination during sample transfer and scanning. Fourier transform infrared (FTIR) spectra were recorded on a Bruker Tensor 27 Fourier Transform Infrared Spectrometer with a resolution of 4 cm^{-1}. All testing samples were first mixed evenly with potassium bromide (KBr) at a weight ratio of 1:150 and then cold-pressed to form a pellet. The transmission mode was adopted and each spectrum was created using 16 scans on the average. ^{11}B NMR spectra were recorded at room temperature by using an Agilent DD2 600MHz spectrometer operating at 192.42 MHz. About 8 mg of samples were dissolved in 0.5 ml of deuterated DMSO (Cambridge Isotope Laboratories) and loaded into 5 mm NMR tubes (NORELL ST500). The NMR tubes were sealed with Kel-F caps inside an Ar-filled glovebox to protect the samples from contacting air. All spectra were obtained after 16 scans with an acquisition time of 1.1796 s per scan and a relaxation time of 1 s. X-ray absorption fine structure (XAFS) measurements at the Co K-edge (7.709 keV) were conducted in transmission mode at room temperature at the 14W1 beamline in Shanghai Synchrotron Radiation Facility (SSRF). Metallic cobalt foil and cobalt monoxide (CoO) were used as reference samples. All samples were pressed into pellets by mixing with LiF powders at a weight ratio of 1:30 under a pressure of 10 MPa, which were subsequently coated with solid wax under an inert atmosphere to prevent oxidation. Co K-edge XAFS spectra were analyzed following the standard procedures using the FEFF code.[36-37] The Fourier transformations from energy to frequency space were derived from k^2-weighted data over the range of 3 to 12 Å^{-1}. Data fitting of the radial structure functions (RSFs) was performed in *R*-space by filtering out the first and second coordination shells.

High-resolution transmission electron microscopy (HRTEM, FEI, Tecnai G2 F20 S-TWIN) was employed to observe the morphology of the sample dehydrogenated at 130 °C. The chemical composition was analyzed by the INCA system, an Oxford energy-dispersive X-ray spectrometer (EDS) attached to the TEM measuring system. The sample was quickly transferred from the glove box to the TEM facilities under a nitrogen atmosphere to protect the powder samples from contacting air during the sample transfer.

Results and discussion

Structural Characteristics of CoO-added $LiBH_4{\cdot}NH_3$-3LiH.

Figure 1 shows the XRD patterns and FTIR spectra of the as-prepared $LiBH_4{\cdot}NH_3$-3LiH-xCoO (x = 0, 0.01, 0.05, 0.10 and 0.15) samples. As shown in Figure 1(a), two phases, $LiBH_4{\cdot}NH_3$ and LiH were unambiguously identified with considerable intensities in the XRD profile of the pristine sample. Meanwhile, a weak diffraction peak at 2ϑ = 16.7º assigned to $Li_4BN_3H_{10}$ was also observed. This observation suggests that there is a chemical reaction between $LiBH_4{\cdot}NH_3$ and LiH, which can be triggered readily by hand milling. Further FTIR analyses confirmed the existence of $LiBH_4{\cdot}NH_3$ and $Li_4BN_3H_{10}$ as indicated by their typical B-H and N-H vibrations (Figure 1(b)). The B-H vibrations belonging to $LiBH_4{\cdot}NH_3$ at 2384, 2289, 2222, 1186 and 1124 cm^{-1}, and the corresponding N-H vibrations at 3383 and 1404 cm^{-1} were clearly observed.[38] In addition, the N-H vibrations of $Li_4BN_3H_{10}$ were also detected at 3300 and 3244 cm^{-1}, although their intensities are quite weak.[39] For the CoO-added samples, the characteristic reflections of $LiBH_4{\cdot}NH_3$ and LiH still dominated the XRD profile, but their intensities were significantly weaker, particularly for the strongest reflection of $LiBH_4{\cdot}NH_3$ at 2ϑ = 24.7º. The diffraction peak of $Li_4BN_3H_{10}$ at 2ϑ = 16.7º was also discernible. Moreover, the CoO phase was clearly observed in the CoO-added sample, and the corresponding reflections gradually intensified as the amount of CoO added was increased. FTIR results showed nearly identical peaks in the sample spectra to the pristine sample. On closer inspection, an additional absorbance at 1099 cm^{-1} was observed, and this peak gradually intensified as the amount of CoO added was increased. This observation can be attributed to the B-H vibration of the BH_4 group in $LiBH_4$. Further NMR examination confirmed the presence of $LiBH_4$ because the ^{11}B resonance peak was detected at -35.44 ppm (Fig. S2, ESI†). This result indicates that the presence of CoO promotes the reaction between $LiBH_4{\cdot}NH_3$ and LiH, which gives rise to the formation of $LiBH_4$. From this, we can conclude that the as-prepared $LiBH_4{\cdot}NH_3$-3LiH sample was composed mainly of $LiBH_4{\cdot}NH_3$ and LiH, with minor amounts of $Li_4BN_3H_{10}$ and $LiBH_4$. As for the CoO-added samples, the CoO was also one of the primary phases present, in addition to $LiBH_4{\cdot}NH_3$, LiH and minor amounts of $Li_4BN_3H_{10}$ and $LiBH_4$.

Dehydrogenation Behaviour of CoO-added $LiBH_4{\cdot}NH_3$-3LiH.

Figure 2 presents the TPD-MS curves of the $LiBH_4{\cdot}NH_3$-3LiH-xCoO (x = 0, 0.01, 0.05, 0.10 and 0.15) composites as a function of temperature. As shown in Figure 2(a), the H_2 signal curve of the $LiBH_4{\cdot}NH_3$-3LiH sample exhibited three distinct peaks at 30-150 °C, 175-360 °C and 360-480 °C, corresponding to the stepwise dehydrogenation process. More importantly, no NH_3 signal was detected up to a temperature of 500 °C during the heating process (Figure 2(b)), indicating the complete suppression of the NH_3 emission in the presence of a sufficient quantity of LiH. After adding CoO, the first-step dehydrogenation remained nearly constant, in addition to slightly reduced intensities. However, the second-step dehydrogenation moved distinctly to lower temperatures, and the third-step was greatly weakened and even disappeared when x > 0.1 in $LiBH_4{\cdot}NH_3$-3LiH-*x*CoO. The peak temperature of the second-step dehydrogenation was reduced from 290 °C (x = 0) to 240 °C (x = 0.01), 210 °C (x = 0.05), 197 °C (x = 0.1) and 188 °C (x = 0.15), respectively. These results show that the addition of a small amount of CoO significantly reduces the operating temperature for the majority of the dehydrogenation. The quantity of hydrogen desorption from the $LiBH_4{\cdot}NH_3$-3LiH-*x*CoO (*x* = 0, 0.01, 0.05, 0.10 and 0.15) composites as a function of temperature was measured by using a volumetric method. The results are shown in Figure 3.

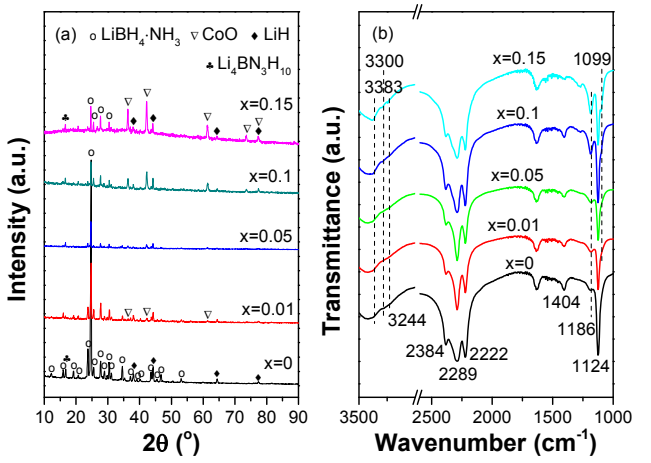

Fig. 1 XRD patterns (a) and FTIR spectra (b) of the as-prepared $LiBH_4{\cdot}NH_3$-3LiH-xCoO composites.

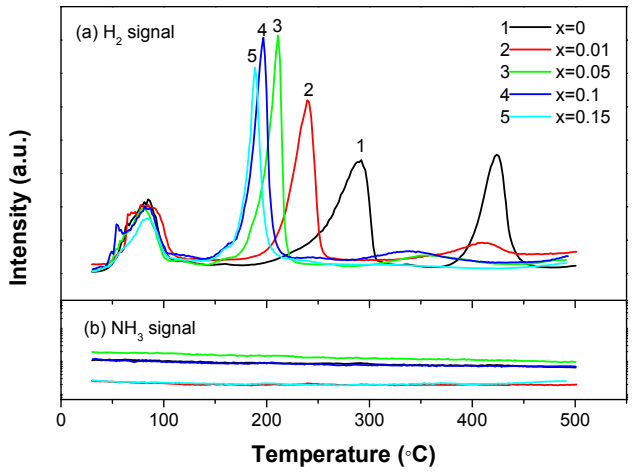

Fig. 2 MS-H_2 signals (a) and NH_3 signals (b) of the $LiBH_4{\cdot}NH_3$-3LiH-xCoO composites as a function of temperature.

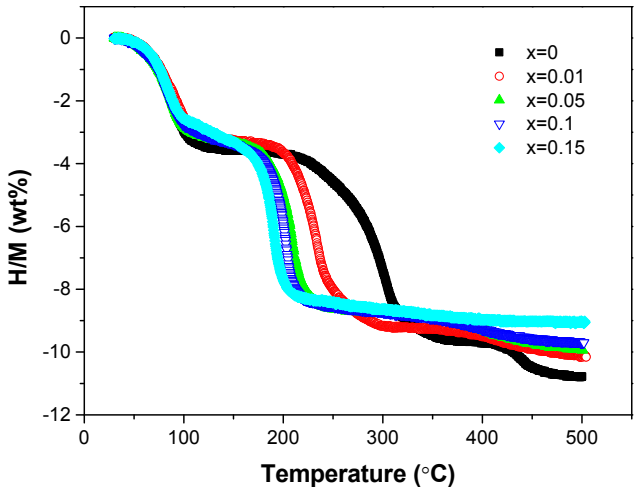

Fig. 3 Volumetric release curves of $LiBH_4{\cdot}NH_3$-3LiH-*x*CoO samples.

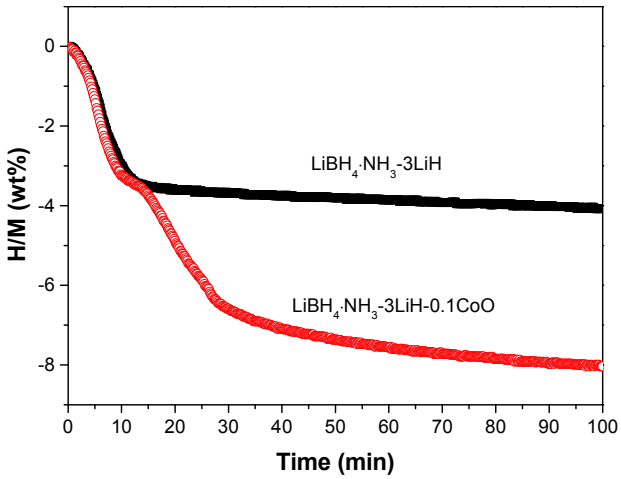

Fig. 4 Isothermal dehydrogenation curves of the $LiBH_4{\cdot}NH_3$-3LiH and $LiBH_4{\cdot}NH_3$-3LiH-0.1CoO samples at 200 ºC.

Hydrogen desorption from the $LiBH_4{\cdot}NH_3$-3LiH sample was detected at the beginning of heating (~ 30 °C), and there are three distinct dehydrogenation steps observed in the volumetric release curve, which is in good agreement with the TPD result (Figure 2(a)). The quantities of hydrogen desorbed were calculated to be 3.6, 6.1 and 1.1 wt% hydrogen for the three steps of dehydrogenation at 30-150 ºC,180-375 ºC and 390-480 ºC, respectively. As a result, hydrogen desorption amounted to 10.8 wt% while heating the $LiBH_4{\cdot}NH_3$-3LiH sample to 500 ºC. After adding 0.01 mol CoO, the operating temperature of the second-step dehydrogenation was significantly reduced, although it remained nearly constant in the first step. The midpoint temperature of the second-step dehydrogenation was reduced from 290 to 235 ºC, exhibiting a 55 ºC reduction with respect to the pristine sample. At the same time, the onset temperature of the third-step dehydrogenation was lowered slightly, accompanied by decrease in the dehydrogenation amount. The hydrogen desorption amounted to 3.3, 5.9 and 0.9 wt% for the three dehydrogenation steps, which delivers a total dehydrogenation of 10.1 wt%. Increasing the amount of added CoO to 0.05 mol, the midpoint temperature of the second-step dehydrogenation was further lowered to 210 ºC, and the total dehydrogenation was decreased to 9.9 wt%. On increasing the amount of CoO added further to 0.1 and 0.15 mol, the dehydrogenation temperature of the second-step exhibited only a slight reduction, while there is a continuous decrease in the dehydrogenation amount for the third-step dehydrogenation. Taking everything into consideration, the addition of 0.1 mol of CoO should be the optimal amount to catalyze the hydrogen desorption from $LiBH_4{\cdot}NH_3$-3LiH in the present study. As shown in Figure 3, the $LiBH_4{\cdot}NH_3$-3LiH-0.1CoO composite released 9.7 wt% hydrogen via a three-step reaction with an onset temperature of 30 ºC. In particular, approximately 8.5 wt% hydrogen was liberated from the $LiBH_4{\cdot}NH_3$-3LiH-0.1CoO composite below 250 ºC, corresponding to 90% of the total dehydrogenation amount. However, only 4.6 wt% hydrogen was released from the additive-free sample under identical conditions.

Dehydrogenation Kinetics and Thermodynamics of CoO-added $LiBH_4{\cdot}NH_3$-3LiH.

Figure 4 presents the isothermal dehydrogenation curves of the composites of $LiBH_4{\cdot}NH_3$-3LiH and $LiBH_4{\cdot}NH_3$-3LiH-0.1CoO at 200 ºC. The results showed significantly improved dehydrogenation kinetics for the CoO-added sample. The $LiBH_4{\cdot}NH_3$-3LiH-0.1CoO sample released 8.0 wt% hydrogen within 100 min at 200 ºC. However, only 4.1 wt% hydrogen was evolved from the pristine sample under identical conditions. Specifically, a 2-fold increase was achieved in the dehydrogenation kinetics by the addition of CoO. Moreover, it should be noted that the isothermal dehydrogenation curve of the $LiBH_4{\cdot}NH_3$-3LiH-0.1CoO sample exhibited two distinct stages. In the first stage, approximately 3.4 wt% of hydrogen was released within 13 min, which overlapped with the dehydrogenation curve of the additive-free sample. With a prolonged dwelling time from 13-100 min, an additional 4.6 wt% of hydrogen was released from the $LiBH_4{\cdot}NH_3$-3LiH-0.1CoO sample. This result further indicated that the addition of CoO significantly improved the dehydrogenation properties of the second-step dehydrogenation. The kinetic barriers for the hydrogen desorption from the $LiBH_4{\cdot}NH_3$-3LiH and $LiBH_4{\cdot}NH_3$-3LiH-0.1CoO systems were further evaluated quantitatively via Kissinger's method as described below.[40]

$$\frac{d\ln(\frac{\beta}{T_m^2})}{d(\frac{1}{T_m})} = -\frac{E_a}{R} \quad (1)$$

Where E_a is the apparent activation energy in kJ mol^{-1}, β is the heating rate in K min^{-1}, T_m is the desorption peak temperature in K, and R is the gas constant. The values of T_m were obtained from the TPD curves collected at heating rates of 2, 3, 5 and 7 K min^{-1}, respectively. Here, the apparent activation energies of the first and second-step dehydrogenation were calculated because only a small amount of hydrogen was released from the $LiBH_4{\cdot}NH_3$-3LiH-0.1CoO sample at 390-480 ºC. As shown in Figure 5(a) and (b), the E_a values of the first and second-step dehydrogenation were approximately 74.0 and 92.5 kJ mol^{-1} for the $LiBH_4{\cdot}NH_3$-3LiH sample, respectively, and they were 70.6 and 53.6 kJ mol^{-1} for the $LiBH_4{\cdot}NH_3$-3LiH-0.1CoO sample.

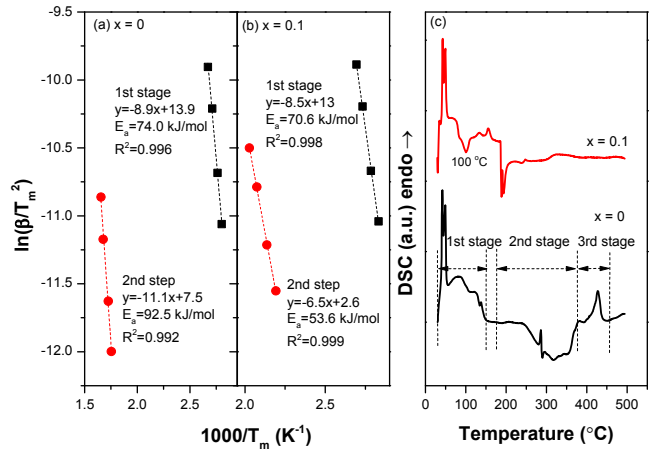

Fig. 5 Kissinger plots (a) and (b) and DSC curves (c) of the $LiBH_4{\cdot}NH_3$-3LiH (x = 0) and $LiBH_4{\cdot}NH_3$-3LiH-0.1CoO (x = 0.1) composites at 2 ºC/min.

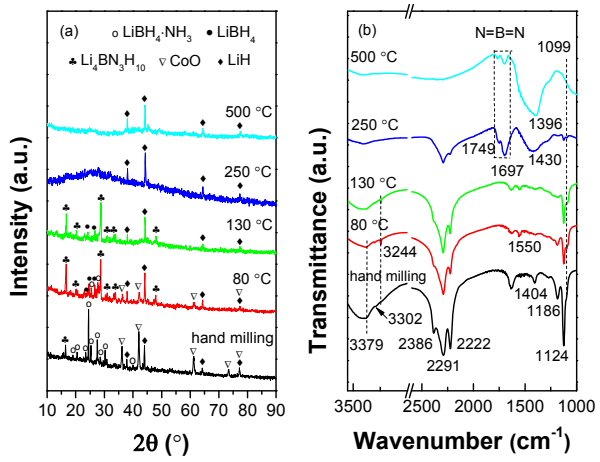

Fig. 6 XRD patterns (a) and FTIR spectra (b) of the dehydrogenated $LiBH_4{\cdot}NH_3$-3LiH-0.1CoO samples.

Clearly, the apparent activation energy of the first-step dehydrogenation remained nearly constant, while it was reduced dramatically for the second-step dehydrogenation with the addition of CoO. This result indicates that the kinetic barriers of the second-step dehydrogenation have been reduced. This is closely related to the reduced operating temperature observed for the second-step dehydrogenation of the $LiBH_4{\cdot}NH_3$-3LiH-0.1CoO sample. Figure 5(c) shows the DSC curves of the $LiBH_4{\cdot}NH_3$-3LiH and $LiBH_4{\cdot}NH_3$-3LiH-0.1CoO samples at 2 ºC min^{-1}. As shown in Figure 5(c), a rather complicated heat-flow behaviour was observed for the $LiBH_4{\cdot}NH_3$-3LiH and $LiBH_4{\cdot}NH_3$-3LiH-0.1CoO samples while heating from room temperature to 500 ºC. The heat events of the $LiBH_4{\cdot}NH_3$-3LiH sample occurred mainly within 30-150, 190-370 and 380-450 ºC, which correspond to the three steps of dehydrogenation as shown in Figs. 2 and 3. As a result, the first and third-steps of dehydrogenation are endothermic in nature, while the second-step dehydrogenation is an exothermic reaction. On comparison, it was clear that the exothermic peak of the second-step dehydrogenation of the CoO-added sample shifted significantly to lower temperatures relative to the pristine sample, providing further evidence that the significantly reduced operating temperatures for the second-step dehydrogenation occurs due to the addition of CoO. Moreover, the endothermic peak of the third-step was distinctly weakened, which consists well with the TPD results as shown in Fig. 2(a). In particular, an additional exothermic event was also detected at 100 ºC for the CoO-added sample, which may be related to a chemical reaction in which CoO is involved. This event explains the reduced operating temperature in the dehydrogenation process well.

Dehydrogenation Mechanisms of CoO-added $LiBH_4{\cdot}NH_3$-3LiH.

To understand the chemical events occurring during the heating process, the dehydrogenated $LiBH_4{\cdot}NH_3$-3LiH-0.1CoO sample at different temperatures were collected for XRD and FTIR analysis. The results are shown in Figure 6. As shown in Figure 6(a), the $Li_4BN_3H_{10}$ and LiH phases were the dominant species present in the XRD profile after dehydrogenation at 80 ºC. However, the characteristic reflections of $LiBH_4{\cdot}NH_3$ nearly disappeared along with a distinct decrease in those of CoO, indicating these species were consumed in the dehydrogenation process. Further examination by FTIR (Figure 6(b)) revealed an obvious change in the relative intensities of the absorbance associated with B-H vibration at 2384, 2289 and 2222 cm^{-1}, which are much closer to the characteristic B-H vibrations in $Li_4BN_3H_{10}$. Moreover, the $LiBH_4$ phase was also detected at 2ϑ = 23.7, 24.6 and 26.7º, although their intensities are weak. This result was further confirmed by FTIR analysis, with a considerably intense absorbance typical of the B-H vibration in $LiBH_4$ observed at 1099 cm^{-1} (Figure 6(b)). From these observations, it is fair to speculate that $LiBH_4{\cdot}NH_3$ reacts with LiH to release hydrogen and converted to $Li_4BN_3H_{10}$ and $LiBH_4$ below 80 ºC when catalyzed by CoO, as described below. Such a reaction temperature range is distinctly lower than that of the pristine $LiBH_4{\cdot}NH_3$-LiH system (60-150 ºC), as reported by Yu et al.[18]

$$LiBH_4{\cdot}NH_3 + 3LiH \xrightarrow{CoO} Li_4BN_3H_{10} + 2LiBH_4 + 3H_2 \quad (2)$$

While the sample was heated to 130 ºC, three phases of $Li_4BN_3H_{10}$, LiH and $LiBH_4$ were discernible in the XRD profile, and the diffraction peaks of $LiBH_4{\cdot}NH_3$ and CoO were completely undetectable. The characteristic absorbance of the B-H vibration in $LiBH_4{\cdot}NH_3$ at 1186 cm^{-1}, and the N-H vibration at 1404 cm^{-1} disappeared. Moreover, it should be mentioned that the diffraction peaks of $Li_4BN_3H_{10}$ shown in Figure 6(a) decreased slightly in comparison to the sample dehydrogenated at 80 ºC. This suggests the decomposition of $Li_4BN_3H_{10}$ commenced. Further elevation of the dehydrogenation temperature to 250 ºC, only the typical reflections of LiH and two bumps centred at 17.2 and 27.6º associated with $LiBH_4$,[41] were detected by means of XRD, accompanied by the disappearance of $Li_4BN_3H_{10}$. The existence of $LiBH_4$ was confirmed by NMR measurement as shown in Fig. S2 (ESI†). Further examination by FTIR revealed that the N-H vibrations at 3200-3400 cm^{-1} were no longer visible, and the B-H vibrations at 2100-2450 and 1050-1150 cm^{-1} were significantly weaker. However, the N-B-N vibrations at 1749 and 1697 cm^{-1}, assigned to Li_3BN_2, and a broad B-N vibration

centred at 1430 cm^{-1}, appeared in the FTIR spectrum.[32] Consequently, it is believed that Li_3BN_2 and BN exist in the 250 ºC-dehydrogenated sample, in addition to LiH. The corresponding reaction process can be written as follows:

$$Li_4BN_3H_{10} + LiBH_4 \rightarrow Li_3BN_2 + BN + 2LiH + 6H_2 \quad (3)$$

After dehydrogenation at 500 ºC, the bumps belonging to $LiBH_4$ disappeared, and only the LiH phase dominated the XRD profile. Moreover, no B-H or N-H vibrations were observed in the FTIR spectrum. It is well known that $LiBH_4$ decomposes to release hydrogen and produce LiH and B above 250 ºC as follows:[42]

$$2LiBH_4 \rightarrow 2LiH + 2B + 3H_2 \quad (4)$$

From the above discussion, the hydrogen desorption process of $LiBH_4{\cdot}NH_3$-3LiH-0.1CoO can be summarized as follows:

$$\begin{aligned} LiBH_4{\cdot}NH_3 + 3LiH &\rightarrow \frac{1}{3}Li_4BN_3H_{10} + \frac{2}{3}LiBH_4 + 2LiH + H_2 \\ &\rightarrow \frac{1}{3}Li_3BN_2 + \frac{1}{3}LiBH_4 + \frac{1}{3}BN + \frac{8}{3}LiH + 3H_2 \\ &\rightarrow \frac{1}{3}Li_3BN_2 + \frac{1}{3}BN + 3LiH + \frac{1}{3}B + \frac{7}{2}H_2 \end{aligned} \quad (5)$$

Theoretically, the hydrogen desorption from this reaction amounts to 11.1 wt%, which is in good agreement with the experimental results shown in Figure 3.

Role Played by Co during Hydrogen Release from CoO-added $LiBH_4{\cdot}NH_3$-3LiH.

Moreover, it should be mentioned that no structural information of Co-containing species was observed by XRD or FTIR for the dehydrogenated samples. To understand the role played by CoO during the dehydrogenation of $LiBH_4{\cdot}NH_3$-3LiH-0.1CoO, XAFS was performed at the Co K-edge, and the XANES spectra are shown in Figure 7(a). Here, the CoO and metallic Co were used as references. The hand-milled sample exhibited an identical XANES spectrum to CoO. This reveals that CoO persists throughout the hand milling process. This is in agreement with the XRD results (Figure 6). After dehydrogenation at 80 ºC, a shoulder appears at lower energy (7712 eV) with a corresponding decrease of the main absorption peak at 7726 eV. This indicates that the local geometry of the Co atoms has changed and that the electronic state of the Co-O bonds has been reduced. While the dehydrogenation temperature was elevated to 130 ºC, the XANES spectrum of the dehydrogenated sample was quite similar to that of metallic Co. This result suggests that the CoO additive was reduced to metallic Co during the initial heating process. Further increasing the dehydrogenation temperature to 250 ºC, the XANES spectrum remains nearly constant, in addition to the appearance of the shoulder at 7712 eV that became more distinct, indicating that a new Co-based species with a different symmetry developed, in addition to the metallic Co in the subsequent dehydrogenation.

Figure 7(b) presents the Fourier transformations of the XAFS spectra of the dehydrogenated $LiBH_4{\cdot}NH_3$-3LiH-0.1CoO samples as a function of temperature. The radial structure functions (RSFs) at the Co-K edge of all samples were derived from the k^2-weighted data over the range of 3 to 12 $Å^{-1}$. For

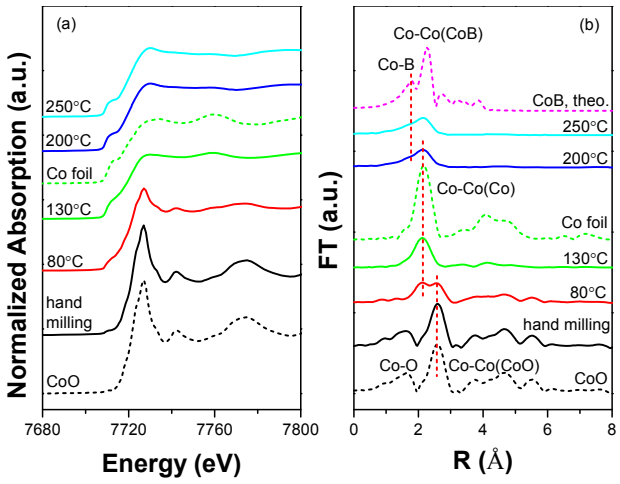

Fig. 7 XANES spectra and Fourier transformations at the Co K-edge of the dehydrogenated $LiBH_4{\cdot}NH_3$-3LiH-0.1CoO samples under various conditions.

comparison, the RSFs of the Co foil and CoO, together with a CoB calculation with the multiple scattering theory using FEFF6, were also included. The phase shift was not corrected. As shown in Figure 7(b), the Fourier transformation of the XAFS spectrum of the hand-milled sample exhibited two dominant peaks at approximately 1.6 and 2.6 Å, which corresponds to the Co-O coordination of the first shell of CoO and the Co-Co coordination of the second shell. This result further confirmed the existence of CoO in the hand-milled sample. In addition, two to three peaks arise from higher-order shells, representing a good crystallinity, *i.e.*, relatively high degree of structural order. After dehydrogenation at 80 ºC, the peak at 1.6 Å was undetectable, along with an obvious reduction in the main peak at 2.6 Å. Meanwhile, a new peak appeared with a considerable intensity at 2.1 Å, which agrees well with the Co-Co coordination in the metallic Co. These observations indicate CoO and metallic Co co-exist in the 80 ºC-dehydrogenated sample. While the sample dehydrogenated at 130 ºC, only the newly developed peak at 2.1 Å was observed in the Fourier transformed spectrum, indicating that only metallic Co existed, which was confirmed by the RSF fitting as shown in Table 1. Moreover, the significantly fewer average coordination numbers of the first Co-Co shell, and the shorter bond length compared to the reference structure, implies that metallic Co should have been formed as very small particles. Further increasing the dehydrogenation temperature to 250 ºC, the dominant peak at 2.1 Å exhibited a distinct asymmetry due to the appearance of a small shoulder at 1.7 Å, which can be assigned to the Co-B coordination in CoB, calculated according to the structural parameters reported previously.[43] Further fitting results confirmed the formation of covalent bonding in Co-B because the Co-B distance was calculated to be 2.13 Å, much shorter than the sum of the atomic radii of Co and B (2.32 Å). From Table 1, it can be seen that certain amounts of CoB co- existed with Co in the sample. In addition, it should be noted that the high-order coordination peaks were absent after dehydrogenation at 250 ºC, indicating a poor crystallinity, which is in good agreement with the XRD results shown in Figure 6. In accordance with our discussions above, we can

Table 1. Structural Parameters of the LiBH4·NH3-3LiH-0.1CoO Dehydrogenated Samples Determined from the Co K-edge EXAFS Spectra.[a]

sample	shell	Coordination	N	R (Å)	σ^2 (Å^2)
CoO	1	Co-O	6	2.13	-
	2	Co-Co	12	3.11	-
Co	1	Co-Co	12	2.51	-
CoB	1	Co-B	14	2.12-2.14	-
Hand-milled sample	1	Co-O	6	2.13	0.0075
	2	Co-Co (CoO)	10.2	3.01	0.0088
Sample dehydrogenated at 80 ºC	1	Co-O	3.1	2.11	0.012
	2	Co-Co (Co)	1.7	2.42	0.011
	3	Co-Co (CoO)	8.7	2.98	0.011
Sample dehydrogenated at 130 ºC	1	Co-Co (Co)	5.7	2.47	0.0073
	2	Co-Co (CoO)	0.2	2.88	0.012
Sample dehydrogenated at 200 ºC	1	Co-B	6.3	2.12	0.0073
	2	Co-Co (Co)	3.3	2.51	0.0094
Sample dehydrogenated at 250 ºC	1	Co-B	7.0	2.13	0.0060
	2	Co-Co (Co)	2.8	2.53	0.010

[a]Error bars for *R* are 0.01 Å, for *N* and σ^2, 10%.

conclude with confidence that the CoO additive was first reduced to give rise to the formation of metallic Co in the initial heating stage, before some of the newly formed Co reacted with B to generate CoB at an elevated temperature. It was recently reported that metallic Co and Co-B species have superior catalytic effects on the thermolytic dehydrogenation of the Li-B-N-H system,[33-35] which is closely responsible for the significant reduction in the operating temperature of the second-step dehydrogenation because it originates from the reaction between $Li_4BN_3H_{10}$ and $LiBH_4$ as described by reaction (2).

Figure 8(a) displays the high-resolution TEM (HRTEM) image of the $LiBH_4$·NH_3-3LiH-0.1CoO sample dehydrogenated at 130 ºC. It was observed that some particles, with diameters ranging from 1.5 to 4 nm, were well dispersed in the amorphous matrix. These fine particles were proven to be the Co-containing species by means of EDS, as shown in Figure 8(b). Such fine particles of Co are consistent with the speculations arising from the EXAFS fitting results, and they reveal why it was not detectable in the XRD profile (Figure 6). Encouragingly, these fine Co particles may provide quite a large specific surface area and consequently have a superior catalytic activity, to significantly reduce the dehydrogenation temperatures of the second-step dehydrogenation. Unfortunately, attempts to hydrogenate the dehydrogenated products failed under 100 bar at 250 ºC. This may be due to the formation of Li_3BN_2 and BN, which are quite stable under mild temperatures and hydrogen pressures.[19]

Conclusions

The dehydrogenation properties of the $LiBH_4$·NH_3-3LiH-xCoO (x = 0-0.15) composites were systematically investigated in this work. It was found that the pristine sample and CoO-added samples all experience three stepwise dehydrogenation stages during their thermal decomposition process. The addition of CoO can significantly reduce the operating temperature of the second reaction stage, as well as the thermodynamic and

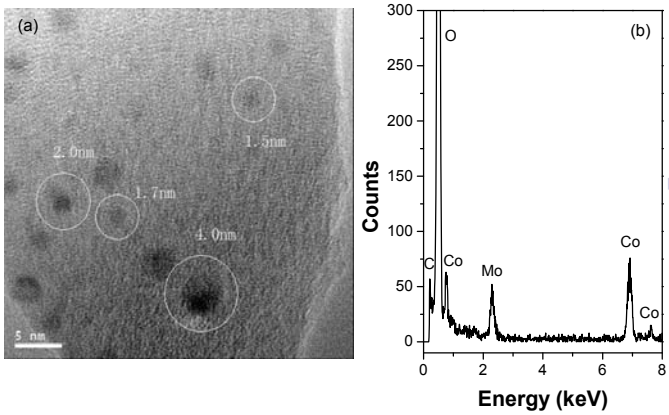

Fig. 8 TEM image (a) and EDS spectrum (b) of the $LiBH_4$·NH_3-3LiH-0.1CoO sample dehydrogenated at 130 ºC.

kinetic barriers of the $LiBH_4$·NH_3-3LiH system. The $LiBH_4$·NH_3-3LiH-0.1CoO system was found to possess the optimal dehydrogenation properties, giving off 8.5 wt% of hydrogen below 250 ºC, approximately 90 ºC lower with respect to the pristine sample. Approximately 8.0 wt% of the hydrogen was released from the CoO-added sample within 100 min at 200 °C. The XAFS analysis revealed that the CoO was first reduced to metallic Co at 130 ºC and then partially combined with B to form a Co-B covalent bond. The Co and Co-B formed *in situ* were found to be finely dispersed in the dehydrogenation intermediates, which play a critical role as the actual active catalyst in decreasing the thermodynamic and kinetic barriers of the dehydrogenation reaction of the $LiBH_4$·NH_3-3LiH system.

Acknowledgements

We gratefully acknowledge the financial support received from the National Natural Science Foundation of China (51171170, 51222101), the Research Fund for the Doctoral Program of Higher Education of China (20130101110080, 20130101130007), the Program for Innovative Research Team at the University of Ministry of Education of China (IRT13037) and the Fundamental Research Funds for the Central Universities (2014XZZX003-08, 2014XZZX005).

References

1 M. A. Pellow, C. J. M. Emmott, C. J. Barnhart and S. M. Benson, *Energy Environ. Sci.*, 2015, DOI:10.1039/c4ee04041d.
2 L. Schlapbach and A. Züttel, *Nature*, 2001, **414**, 353.
3 G. Cipriani, V. Di Dio, F. Genduso, D. La Cascia, R. Liga, R. Miceli and G. R. Galluzzo, *Int. J. Hydrogen Energy*, 2014, **39**, 8482.
4 M. B. Ley, L. H. Jepsen, Y. S. Lee, Y. W. Cho, J. M. B. von Colbe, M. Dornheim, M. Rokni, J. O. Jensen, M. Sloth, Y. Filinchuk, J. E. Jørgensen, F. Besenbacher and T. R. Jensen, *Mater. Today*, 2014, **17**, 122.
5 J. H. Wang, H. W. Li and P. Chen, *MRS Bull.*, 2013, **38**, 480.
6 L. Li, C. C. Xu, C. C. Chen, Y. J. Wang, L. F. Jiao and H. T. Yuan, *Int. J. Hydrogen Energy*, 2013, **38**, 8798.
7 A. Züttel, P. Wenger, S. Rentsch, P. Sudan, Ph. Mauron and Ch. Emmenegger, *J. Power Sources*, 2003, **118**, 1.
8 K. Chlopek, C. Frommen, A. Leon, O. Zabara and M. Fichtner, *J. Mater. Chem.*, 2007, **17**, 3496.

9 J. J. Hu, R. Witter, H. Y. Shao, M. Felderhoffc and M. Fichtner, *J. Mater. Chem. A*, 2014, **2**, 66.
10 H. Grove, L. H. Rude, T. R. Jensen, M. Corno, P. Ugliengo, M. Baricco, M. H. Sørby and B. C. Hauback, *RSC Adv.*, 2014, **4**, 4736.
11 B. Bogdanovic and M. Schwickardi, *J. Alloys Compd.*, 1997, **253-254**, 1.
12 X. Zhang, Y. F. Liu, Y. P. Pang, M. X. Gao and H. G. Pan, *J. Mater. Chem. A*, 2014, **2**, 1847.
13 X. Zhang, Y. F. Liu, K. Wang, M. X. Gao and H. G. Pan, *Nano Res.*, 2015, **8**, 533.
14 P. Chen, Z. T. Xiong, J. Z. Luo, J. Y. Lin and K. L. Tan, *Nature*, 2002, **420**, 302.
15 Z. T. Xiong, G. T. Wu, J. J. Hu, Y. F. Liu, P. Chen, W. F. Luo and J. Wang, *Adv. Funct. Mater.*, 2007, **17**, 1137.
16 S. Orimo, Y. Nakamori, G. Kitahara, K. Miwa, N. Ohba, S. Towata and A. Züttel, *J. Alloys Compd.*, 2005, **404-406**, 427.
17 A. Züttel, A. Borgschulte and S. I. Orimo, *Scr. Mater.*, 2007, **56**, 823.
18 X. B. Yu, Y. H. Guo, D. L. Sun, Z. X. Yang, A. Ranjbar, Z. P. Guo, H. K. Liu and S. X. Dou, *J. Phys. Chem. C*, 2010, **114**, 4733.
19 F. E. Pinkerton, G. P. Meisner, M. S. Meyer, M. P. Balogh and M. D. Kundrat, *J. Phys. Chem. B*, 2005, **109**, 6.
20 H. Wu, W. Zhou and T. Yildirim, *J. Am. Chem. Soc.*, 2008, **130**, 14834.
21 Z. T. Xiong, C. K. Yong, G. T. Wu, P. Chen, W. Shaw, A. Karkamkar, T. Autrey, M. O. Jones, S. R. Johnson, P. P. Edwards and W. I. F. David, *Nat. Mater.*, 2008, **7**, 138.
22 G. Soloveichik, J.-H. Her, P. W. Stephens, Y. Gao, J. Rijssenbeek, M. Andrus and J.-C. Zhao, *Inorg. Chem.*, 2008, **47**, 4290.
23 Y. H. Guo, X. B. Yu, W. W. Sun, D. L. Sun and W. N. Yang, *Angew. Chem. Int. Ed.*, 2011, **50**, 1087.
24 X. W. Chen and X. B. Yu, *J. Phys. Chem. C*, 2012, **116**, 11900.
25 Y. Z. Song, F. L. Wu, X. F. Zheng, X. H. Ma, F. Fang and Y. H. Guo, *Chem. Commun.*, 2015, **51**, 1104.
26 Y. J. Yang, Y. F. Liu, Y. Li, M. X. Gao and H. G. Pan, *J. Mater. Chem. A*, 2015, **3**, 570.
27 D. J. Hunt and P. A. Cowie, Summary Report XXXI, Sub-contract No.M-3181-14, St. Louis University, 1955.
28 S. R. Johnson, W. I. F. David, D. M. Royse, M. Sommariva, C. Y. Tang, F. P. A. Fabbiani, M. O. Jones and P. P. Edwards, *Chem. Asian J.*, 2009, **4**, 849.
29 X. L. Zheng, G. T. Wu, W. Li, Z. T. Xiong, T. He, J. P. Guo, H. Chen adn P. Chen, *Energy Environ. Sci.*, 2011, **4**, 3593.
30 X. Y. Chen, W. Y. Cai, Y. H. Guo and X. B. Yu, *Int. J. Hydrogen Energy*, 2012, **37**, 5817.
31 S. F. Li, W. W. Sun, Z. W. Tang, Y. H. Guo and X. B. Yu, *Int. J. Hydrogen Energy*, 2012, **37**, 3328.
32 Y. H. Guo, W. W. Sun, Z. P. Guo, H. K. Liu, D. L. Sun and X. B. Yu, *J. Phys. Chem. C*, 2010, **114**, 12823.
33 W. S. Tang, G. T. Wu, T. Liu, A. T. S. Wee, C. K. Yong, Z. T. Xiong, A. T. S. Hor and P. Chen, *Dalton Trans.*, 2008, **18**, 2395.
34 Y. Zhang, Y. F. Liu, T. Liu, M. X. Gao and H. G. Pan, *Int. J. Hydrogen Energy*, 2013, **38**, 13318.
35 Y. Zhang, Y. F. Liu, Y. P. Pang, M. X. Gao and H. G. Pan, *J. Mater. Chem. A*, 2014, **2**, 11155.
36 A. L. Ankudinov and J. J. Rehr, *Phys. Rev. B*, 1997, **56**, R1712.
37 S. I. Zabinsky, J. J. Rehr, A. Ankudinov, R. C. Albers and M. J. Eller, *Phys. Rev. B*, 1995, **52**, 2995.
38 Y. H. Guo, G. L. Xia, Y. H. Zhu, L. Gao and X. B. Yu, *Chem. Commun.*, 2010, **46**, 2599.
39 P. A. Chater, W. I. F. David, S. R. Johnson, P. P. Edwards and P. A. Anderson, *Chem. Commun.*, 2006, **23**, 2439.
40 H. E. Kissinger, *Anal. Chem.*, 1957, **29**, 1702.
41 Y. F. Zhou, Y. F. Liu, Y. Zhang, M. X. Gao and H. G. Pan, *Dalton Trans.*, 2012, **41**, 10980.
42 A. Züttel, S. Rentsch, P. Fischer, P. Wenger, P. Sudan, Ph. Mauron and Ch. Emmenegger, *J. Alloys Compd.*, 2003, **356**, 515.
43 D. Hohnke and E. Parthé, *Acta Cryst.*, 1966, **20**, 572.

Graphical contents entry:

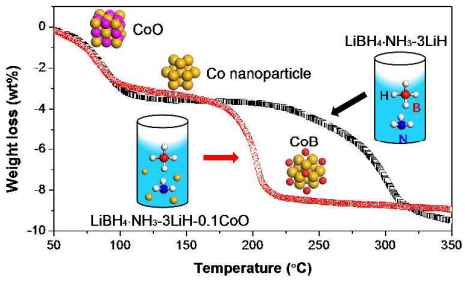

The addition of CoO significantly reduces the dehydrogenation temperature and accelerates the dehydrogenation rate of the $LiBH_4 \cdot NH_3$-3LiH system.